J. Fluid Mech. (2004), *vol.* 520, *pp.* 135–156.
DOI: 10.1017/S0022112004001156 Printed in the United Kingdom

Time-dependent flows in an emptying filling box

By N. B. KAYE AND G. R. HUNT

Department of Civil and Environmental Engineering, Imperial College of Science, Technology and Medicine, Imperial College Road, London, SW7 2AZ, UK

(Received 5 January 2004 and in revised form 28 July 2004)

We examine the transient buoyancy-driven flow in a ventilated filling box that is subject to a continuous supply of buoyancy. A rectangular box is considered and the buoyancy input is represented as a turbulent plume, or as multiple non-interacting plumes, rising from the floor. Openings in the base and top of the box link the interior environment with a quiescent exterior environment of constant and uniform density. A theoretical model is developed to predict, as functions of time, the density stratification and the volume flow rate through the openings leading to the steady state. Comparisons are made with the results of small-scale analogue laboratory experiments in which saline solutions and fresh water are used to create density differences. Two characteristic timescales are identified: the filling box time (T_f), proportional to the time taken for fluid from a plume to fill a closed box; and the draining box time (T_d), proportional to the time taken for a ventilated box to drain of buoyant fluid. The timescale for the flow to reach the steady state depends on these two timescales, which are functions of the box height H and cross-sectional area S, the 'effective' opening area A^*, and the strength, number and distribution of the buoyancy inputs. The steady-state flow is shown to be characterized by the ratio of these timescales ($\mu = T_d/T_f$) which is equivalent to the dimensionless vent area A^*/H^2. A feature of these flows is that for $\mu > \mu_c$ the depth of the buoyant upper layer may exceed, or 'overshoot', the steady layer depth during the initial transient. The value of μ_c is determined for both line and point-source plumes, and the sensitivity of the developing flow to the distribution of buoyancy input assessed.

1. Introduction

We examine the transient flow induced by a semi-confined turbulent plume. The term 'semi-confined' is used here to describe a situation where the flow in the plume develops within a box, but the ambient fluid within the box is free to exchange with an external environment through connections or vent openings. 'Fully confined' plumes were examined by Baines & Turner (1969) in their 'filling box' paper. In a filling box the plume rises to the top of the box and spreads out laterally to form a density interface between the plume outflow and the ambient fluid. Over time this interface descends towards the plume source as ambient fluid is entrained into the plume and passes into the buoyant upper layer. They showed that the time for the box to fill with buoyant fluid scaled on the floor area (S) and height (H) of the box, and the buoyancy flux (B) of the plume. This resulted in the 'filling time', T_f, of

$$T_f \propto \frac{S}{B^{1/3}H^{2/3}}. \tag{1.1}$$

The authors also made predictions of the form of the vertical density stratification in the box at large times. This work was extended by Worster & Huppert (1983) who predicted the transient stratification within the box.

Ventilated boxes were investigated by Linden, Lane-Serff & Smeed (1990) who looked at the transient draining of a box filled with fluid of buoyancy g' relative to the external ambient. The fluid in the box is connected to the external ambient through vents in its top and base. They showed that the time taken to flush the box scaled on the box floor area and height, the area of the two vents and the initial buoyancy of the internal fluid. This led to the 'draining time', T_d, of

$$T_d \propto \frac{S}{A^*}\left(\frac{H}{g'}\right)^{1/2} \tag{1.2}$$

where $g' = g\Delta\rho/\rho$ is the reduced gravity of the buoyant layer, $\Delta\rho$ the density contrast between the layers, ρ the density of the external ambient and A^* the 'effective' area of the upper and lower openings such that

$$a_b^* = 2^{1/2}c_b a_b, \quad a_t^* = 2^{1/2}c_t a_t \tag{1.3}$$

and

$$\frac{1}{A^{*2}} = \frac{1}{a_b^{*2}} + \frac{1}{a_t^{*2}} \tag{1.4}$$

where a_b and a_t denote the areas of the base and top openings, respectively. The symbols c_b and c_t denote the loss coefficients associated with flow through the bottom and top openings, respectively. Note that (1.4) is valid if a_b is greater than or roughly equal to a_t. If the upper opening (assuming positively buoyant plumes) is significantly larger than the base opening then there is the possibility of exchange flow through the upper opening. We restrict our model to situations where the flow is unidirectional in each vent. For high Reynolds number flows c_b and c_t are normally assumed constant ($\approx$0.6). However, Hunt & Holford (2000) and Holford & Hunt (2001) show that the coefficients exhibit a density dependence. For simplicity we assume herein that $c_b = c_t = 0.6$.

Linden *et al.* (1990) combine their draining theory with a filling-box model and examine 'emptying filling boxes'. The case they examine is that of a single buoyant point-source plume in a ventilated box. In this case a steady state is reached in which there is a two-layer stratification. The upper buoyant layer drives a draining flow through the vents. This flow is then balanced by the filling flow from the plume. In the steady state the upper layer depth ($H-h$) depends only on the vent area, the box height and the plume entrainment coefficient (α):

$$\frac{A^*}{H^2C^{3/2}} = \frac{\zeta_{ss}^{5/2}}{\sqrt{1-\zeta_{ss}}} \tag{1.5}$$

where the subscript ss denotes steady state, C is given by

$$C = \pi\left(\frac{5}{2\pi\alpha}\right)^{1/3}\left(\frac{6\alpha}{5}\right)^{5/3} \tag{1.6}$$

for an axisymmetric plume with Gaussian profiles and $\zeta = h/H$. The entire problem can therefore be regarded as geometric, with the steady-state interface height being a function of the box geometry only. This work was extended by Cooper & Linden (1996) and Linden & Cooper (1996) for the case of two and multiple localized sources of buoyancy of different strengths. Additional work on such emptying filling boxes

includes Sandberg & Lindstrom (1990) who looked at forced flow through the box, and Gladstone & Woods (2001) who looked at flow driven by a distributed buoyancy source.

In this paper we re-interpret the parameter $A^*/H^2C^{3/2}$ in (1.5) as being the ratio of the two competing timescales T_d and T_f, and examine the influence of these two times on the transient development of the flow. We begin by developing a theoretical model of the transients (§ 2) and then compare this with the results of analogue laboratory experiments (§ 3). Conclusions are drawn in § 4.

2. Plumes in a ventilated box

We consider the transient buoyancy-driven flow and density stratification induced by the introduction of continuous sources of buoyancy at floor level in a rectangular box of height H and uniform cross-sectional area S (independent of height). Ventilation openings, of area a_b and a_t, made in the base and top of the box, respectively, connect the interior environment to a quiescent exterior environment of constant density ρ. We consider a buoyancy input from n equal non-interacting, localized sources of buoyancy flux B, and that buoyancy transfers between the fabric of the box and the fluid in the interior are negligibly small.

The turbulent plumes that develop above the buoyancy sources entrain ambient fluid as they rise, and on reaching the top, spread radially outwards to form a buoyant layer separated from the ambient layer below by a density interface. Following Baines & Turner (1969) we ignore the outward motion from the plumes and assume that an infinitesimally thin layer forms at time $t = 0$. In practice a layer of non-zero depth forms as a result of the radial outflows from the plumes. Our experiments indicate that this initial layer thickness ($\approx 0.1H$)† scales on the plume width at $z = H$. As the layer depth increases, the interface descends towards the plume source and, hence, the layer is fed with increasingly buoyant fluid. Since the exterior fluid remains unaffected, the pressure difference between the upper and lower levels on the inside becomes less than the pressure difference between the upper and lower levels on the outside. This developing hydrostatic pressure difference drives buoyant fluid out through the upper openings and draws an equal volume of ambient fluid in through the lower openings. The flow through each opening is assumed to be unidirectional. We also assume that mixing between the incoming fluid and the buoyant layer is negligible and that a displacement flow is thereby established and maintained. The volume flux of the outflow increases as the layer becomes deeper and more buoyant and this flux begins to balance the volume flux fed into the buoyant layer by the plumes. After a finite time, a steady-state flow is approached in which the volume fluxes balance, the level of the interface is constant and the stratification consists of two homogeneous layers as confirmed in the experiments of Linden *et al.* (1990). Figure 1 shows schematics of the transient and steady flow.

† This measurement of the plume outflow thickness is considerably less than the $0.25H$ reported in the literature (see Manins 1979; Wong, Griffiths & Hughes 2001). We believe that this is due to the experimental technique used to measure the thickness. Our experiments measured the outflow depth using a dye attenuation technique, so only the buoyant portion of the outflow was measured. Wong *et al.* (2001) measured the outflow thickness by examining the deflection of a vertical line of dye. This latter technique provides a measure of the buoyant outflow depth including the depth of any radial ambient flow induced by shear. As we are concerned with the development of the buoyant layer in this work, we will use our measurements of outflow thickness.

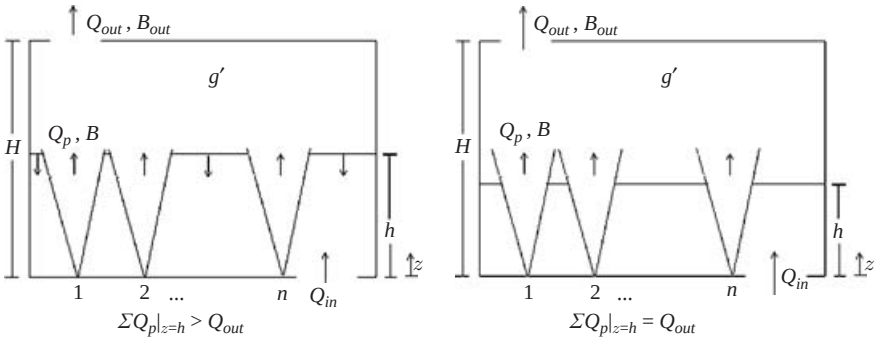

FIGURE 1. Schematics of a ventilated box containing non-interacting localized heat sources of equal strength, showing the density interface: (*a*) descending during the initial transient and (*b*) at steady state when the plume volume flow rate ($\Sigma Q_p|_{z=H}$) balances the outflow (Q_{out}).

For the purposes of modelling the movement of the density interface we assume that the buoyant upper layer is well-mixed during the transient as well as in the steady state. Although one might expect a transient stratification similar to that of a filling box we assume a well-mixed layer. Two points related to this assumption are noted. First, the outflow from the plume is of finite thickness of order a tenth of the height of the box. The dynamics of the finite thickness outflow tends to cause some mixing of the buoyant upper layer, resulting in a more uniform distribution of buoyancy. Second, the flow through the box is driven by the pressure difference between the inside and outside induced by the buoyant layer. This pressure distribution is related to the integral of the buoyancy over the depth of the layer. Therefore, for the purposes of our model, the well-mixed assumption is similar to using top-hat profiles when modelling plumes. The only source of error expected is that our model will tend to underpredict the buoyancy of the fluid flowing out of the box. This will in turn lead to an underprediction of the time taken for the buoyancy of the layer to reach a steady state.

2.1. *Transient model for flow in a ventilated box*

The rate of change in the depth $(H - h)$ of the buoyant layer is determined by the difference between the volume flow rate at which buoyant fluid is supplied (nQ_p) to the upper layer via the n rising thermal plumes, and the volume flow rate at which buoyant fluid drains out through the upper openings (Q_{out}). By conservation of volume, this may be expressed as

$$\frac{\mathrm{d}V}{\mathrm{d}t} = nQ_p - Q_{out} \tag{2.1}$$

where $V = S(H - h)$ is the volume of the buoyant layer. Conservation of buoyancy for the upper layer requires that

$$\frac{\mathrm{d}Vg'}{\mathrm{d}t} = nB - B_{out} \tag{2.2}$$

where g' is the mean buoyancy of the upper layer, and $B_{out} = g'Q_{out}$ is the flux of buoyancy out through the top openings. Note that we are assuming that there are no buoyancy gains or losses through the box walls.

The volume flux Q_p and buoyancy g'_p of a turbulent plume can be written in terms of powers of the buoyancy flux B, the height z above the source, a lengthscale L associated with the source, and a constant C_k that is a function of the plume

entrainment coefficient and source geometry. In the most general form this yields

$$Q_p = C_k B^i z^j L^k, \tag{2.3}$$

$$g'_p = \frac{B}{Q_p} = C_k^{-1} B^{1-i} z^{-j} L^{-k} \tag{2.4}$$

(see Appendix A).

It is now possible to write equations for the time rate of change of the buoyant layer depth $(H-h)$ and of the average layer buoyancy (g') using the plume flow rate scalings given above, and the draining theory outlined by Linden *et al.* (1990):

$$\frac{\mathrm{d}}{\mathrm{d}t}(H-h) = \frac{1}{S}\left(nC_k B^{1/3} h^j L^k - A^* \sqrt{g'(H-h)}\right), \tag{2.5}$$

$$\frac{\mathrm{d}}{\mathrm{d}t}(g'(H-h)) = \frac{1}{S}\left(nB - g' A^* \sqrt{g'(H-h)}\right). \tag{2.6}$$

We now introduce the non-dimensional interface height ζ and reduced gravity δ:

$$h = \zeta H, \quad g' = \delta C_k^{-1} B^{2/3} H^{-j} L^{-k}. \tag{2.7}$$

Equations (2.5) and (2.6) can now be re-written as

$$\frac{\mathrm{d}\zeta}{\mathrm{d}t} = \frac{1}{T_d}\sqrt{\delta(1-\zeta)} - \frac{1}{T_f}\zeta^j, \tag{2.8}$$

$$\frac{\mathrm{d}\delta}{\mathrm{d}t} = \frac{1}{T_f}\left(\frac{1-\zeta^j\delta}{1-\zeta}\right), \tag{2.9}$$

respectively, where the timescales T_d and T_f are defined as

$$T_d = \frac{C_k^{1/2} L^{k/2} S H^{(j+1)/2}}{A^* B^{1/3}} \equiv \frac{S}{A^*}\left(\frac{H}{g'_p|_{z=H}}\right)^{1/2}, \tag{2.10}$$

$$T_f = \frac{S}{nC_k B^{1/3} H^{j-1} L^k} \tag{2.11}$$

which is equivalent to (1.1). The timescale T_d is the 'draining box' time and is proportional to the time taken for a buoyant layer of depth H and of buoyancy equal to that in the plumes at height H to drain completely through openings of effective area A^* (see Linden *et al.* 1990). T_f is the 'filling box' timescale for n non-interacting plumes each of buoyancy flux B (see Baines & Turner 1969). In other words, T_d relates to the draining of a ventilated box in the absence of a supply of buoyancy and T_f relates to the filling of an unventilated box supplied with a constant buoyancy flux from sources at floor level.

We can now fully non-dimensionalize equations (2.8) and (2.9) to obtain

$$\frac{\mathrm{d}\zeta}{\mathrm{d}\tau} = \frac{1}{\sqrt{\mu}}\sqrt{\delta(1-\zeta)} - \sqrt{\mu}\zeta^j, \tag{2.12}$$

$$\frac{\mathrm{d}\delta}{\mathrm{d}\tau} = \sqrt{\mu}\frac{1-\zeta^j\delta}{1-\zeta} \tag{2.13}$$

where the non-dimensional timescale τ and parameter μ are given by

$$t = \tau\sqrt{T_d T_f} = \tau\left(\frac{S^2}{nC_k^{1/2}A^* B^{2/3}L^{k/2}H^{(j-3)/2}}\right)^{1/2}, \tag{2.14}$$

$$\mu = \frac{T_d}{T_f} = \frac{nC_k^{3/2}L^{3k/2}H^{(3j-1)/2}}{A^*}. \tag{2.15}$$

This non-dimensionalization reduces the entire problem to a single parameter μ for a given choice of plume geometry (j, k). The parameter μ is the ratio of the competing timescales for draining and filling the box. For small μ, $T_d < T_f$ and the time taken to drain the box is small compared to the time taken for the plumes to stratify (or fill) the box. For large values of μ the filling time is smaller so the buoyant layer will grow to a significant depth before the draining flow can balance the plumes' input. We would therefore expect that for larger μ it is possible that the buoyant layer will thicken at such a rate that it reaches the steady-state interface height before the draining flow can balance the filling flow. The buoyant layer thickness will therefore overshoot this steady-state thickness. For smaller μ this overshoot will either be less pronounced or disappear. Our numerical results indicate that there is a critical value μ_c above which overshoot occurs. For a given cross-sectional area and height, μ is small for large vent openings and large for small vent openings. When multiple plumes are present, then for a given box geometry, μ increases linearly with the number of plume sources. Also, μ is independent of B. This means that varying B will not affect the steady-state interface height or the extent of any overshoot, only the time taken to reach each height. The steady-state height is a function only of the box geometry (A^*, H) and the number and geometry of the plume sources (n, C_k, j, k) (see Linden *et al.* 1990; Cooper & Linden 1996).

We can compare our model for the transient flow ((2.12) and (2.13)) with that of Linden *et al.* (1990) by looking at the steady-state solution. In the steady state, both time-derivative terms are zero and it is possible to solve for the buoyancy of the upper layer:

$$\delta_{ss} = \zeta_{ss}^{-j} \tag{2.16}$$

and then the layer thickness

$$\frac{1}{\mu^2} = \frac{\zeta_{ss}^{3j}}{1-\zeta_{ss}}. \tag{2.17}$$

Examining the case of n point source plumes, for which $j = \frac{5}{3}$, (2.17) becomes

$$\frac{1}{\mu^2} = \frac{\zeta_{ss}^5}{1-\zeta_{ss}} = \left(\frac{A^*}{nH^2C_0^{3/2}}\right)^2 \tag{2.18}$$

which is identical to the result of equation (2.12) in Linden *et al.* (1990).

In the limit of large μ, $\zeta \to 0$ and the steady-state height can be approximated by

$$\zeta_{ss} = \mu^{-2/3j}. \tag{2.19}$$

This result is used to verify the validity of numerical solutions of the transient flow equations presented later.

2.2. *Initial transient*

For the case of an interior initially at ambient density, we take the time $\tau = 0$ as the moment when the plumes first touch the top of the box. The initial conditions are

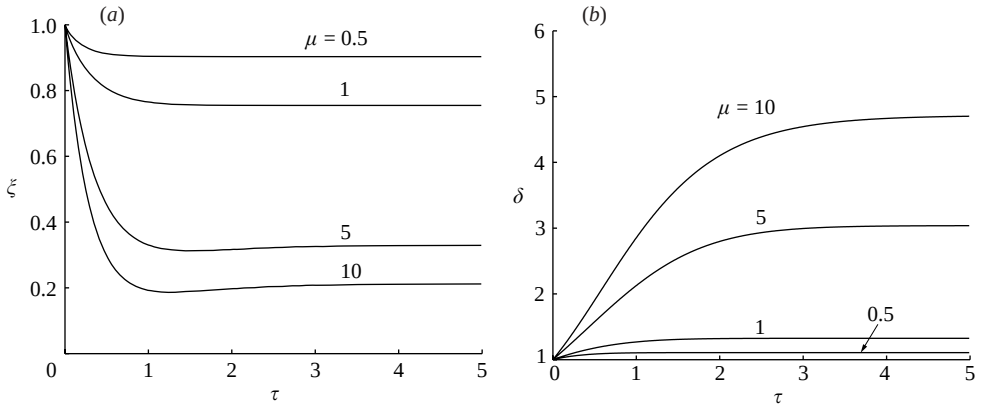

FIGURE 2. Line plumes in a ventilated box with $\mu = \{0.5, 1, 5, 10\}$. (*a*) ζ as a function of τ and (*b*) δ as a function of τ.

therefore

$$\delta = 1, \quad \zeta = 1 \quad \text{at} \quad \tau = 0. \tag{2.20}$$

Solution of the full set of equations (2.12), (2.13) subject to (2.20) was achieved numerically using a simple finite-differencing scheme. To do this, the values of the time derivatives at $\tau = 0$ were required. Clearly $\mathrm{d}\zeta/\mathrm{d}\tau = -\sqrt{\mu}$ at $\tau = 0$ (from (2.12)), and we find that $\mathrm{d}\delta/\mathrm{d}\tau = \frac{1}{2} j \sqrt{\mu}$ (see Appendix B).

Numerical solutions were evaluated for $10^{-3} < \mu < 10^5$ from $\tau = 0$ to $\tau = 50$. This finishing time resulted in the interface height reaching a steady state for the full range of μ considered. It is reasonable to expect that the steady state would be approached, but never reached. However, given the large finish time of $\tau = 50$ the flow approached close enough to the steady state of (2.17) to be graphically indistinguishable.

The key parameters we consider in this model are: the interface height at peak layer depth (maximum overshoot) (ζ_{over}) and at steady state (ζ_{ss}), the layer buoyancy at peak depth (δ_{over}) and steady state (δ_{ss}), and the time taken to reach the peak depth (τ_{over}) and steady state ($\tau_{ss,l}$). The time taken to reach the steady-state layer depth is defined as the time taken ($\tau_{ss,l}$) for the ambient *layer* to reach 99% of its steady-state depth ($|\zeta - \zeta_{ss}| < 0.01$). We later compare this with $\tau_{ss,b}$, the time taken for the layer *buoyancy* to reach 99% of the steady-state value (see figure 10). In the case where the interface overshoots the steady state, $\tau_{ss,l}$ is the time taken to overshoot and then settle back to 99% of the steady-state interface height. $\tau_{ss,l}$ was calculated in order to verify that the choice of timescale was appropriate. The steady-state interface height values ($\zeta_{ss}(\mu)$) were compared with the theoretical values given by (2.17) to check the accuracy of the numerical scheme. The numerical results are shown in figures 2 to 11. Note that many of these figures are plotted on log – log scales so that greater detail can be seen for small μ.

We also examine the conditions under which the buoyant layer depth exceeds the predicted steady-state value during the transient. The range of μ values for which this 'overshoot' occurs is evaluated. A critical value μ_c is introduced (and determined in § 2.3) such that for $\mu > \mu_c$ overshoot is predicted.

Figures 2 and 3 show typical profiles of ζ and δ as a function of τ for line and point-source plumes, respectively. They show the deepening of the buoyant layer over time, including the overshoot. The initial rate of change of the buoyant layer

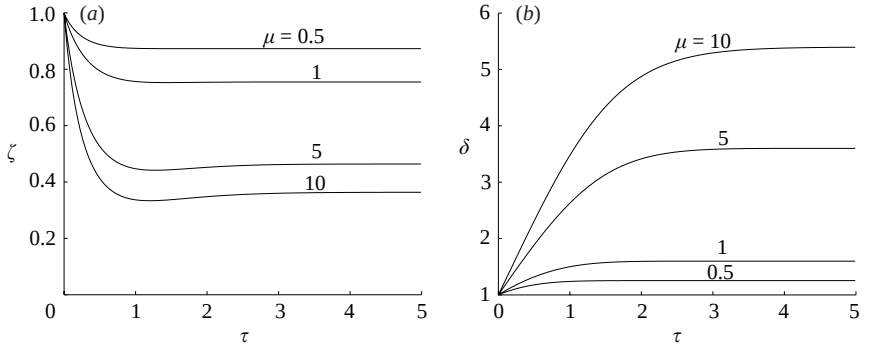

FIGURE 3. Point-source plumes in a ventilated box with $\mu = \{0.5, 1, 5, 10\}$. (*a*) ζ as a function of τ and (*b*) δ as a function of τ.

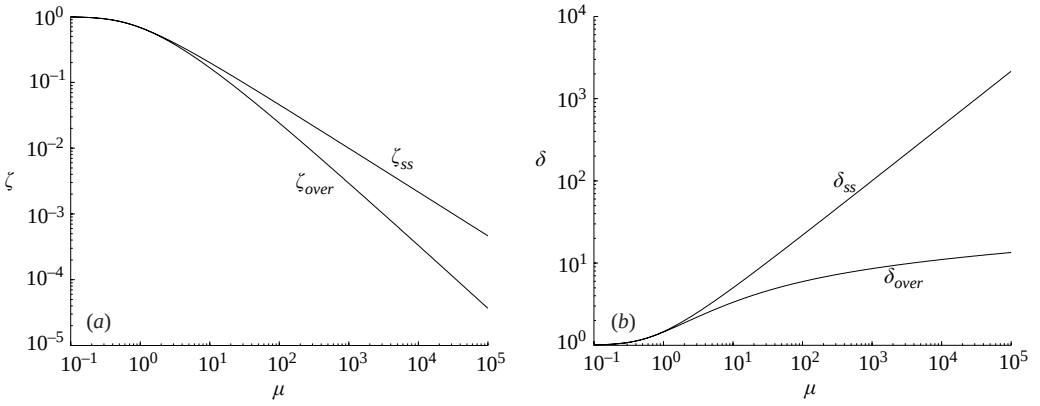

FIGURE 4. Plots of (*a*) ζ_{over}, ζ_{ss}, and (*b*) δ_{over} and δ_{ss}, for a line plume, as a function of μ.

increases with increasing μ. The initial increase in layer depth results in the layer being supplied with increasingly buoyant fluid from the plumes, and a corresponding increase in the buoyancy of the layer. Comparing the steady-state interface heights it is clear that the line plume produces a deeper layer than the equivalent-strength point-source plume. This is due to the greater volume flow rate in the line plume (note that $\zeta > \zeta^{5/3}$ for $\zeta < 1$ comparing (A 4) and (A 5)). At any given height the line plume has a lower buoyancy than an equivalent plume above a point source. The steady-state layer depth required to balance this flow will therefore need to be greater for the line plume, yielding deeper layers.

Figures 4(*a*) and 5(*a*) show the steady state ζ_{ss} and the peak ζ_{over} plotted against μ for line and point-source plumes, respectively. As expected, the value of ζ_{ss} decreases from close to unity for small μ, to close to zero for large μ. This trend is shown for both point-source and line plumes. For values of μ which do not result in overshoot, i.e. $\mu < \mu_c$ (as determined in § 2.3), $\zeta_{over} = \zeta_{ss}$. For $\mu > \mu_c$ the values of ζ_{over} are again lower for each value of μ for line plumes compared to point-source plumes. Figures 4(*b*) and 5(*b*) show δ_{ss} and δ_{over} (the buoyancy at the time of maximum overshoot). For $\mu < \mu_c$, $\delta_{over} = \delta_{ss}$; therefore, when the layer depth increases to the steady-state value, the outflow volume and buoyancy fluxes driven by the buoyant layer exactly match the rate of supply of volume and buoyancy from the plumes so that no overshoot occurs. For larger μ the buoyancy of the layer is clearly lower than the

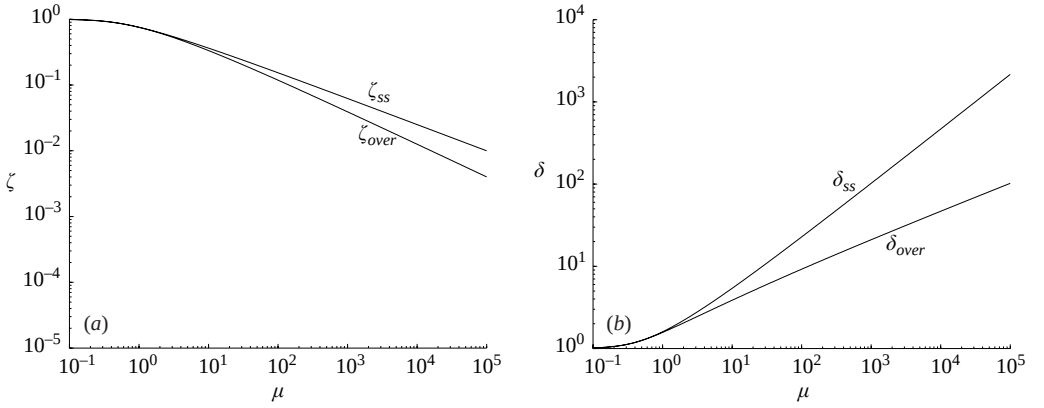

FIGURE 5. Plots of (*a*) ζ_{over}, ζ_{ss}, and (*b*) δ_{over} and δ_{ss}, for a point-source plume, as a function of μ.

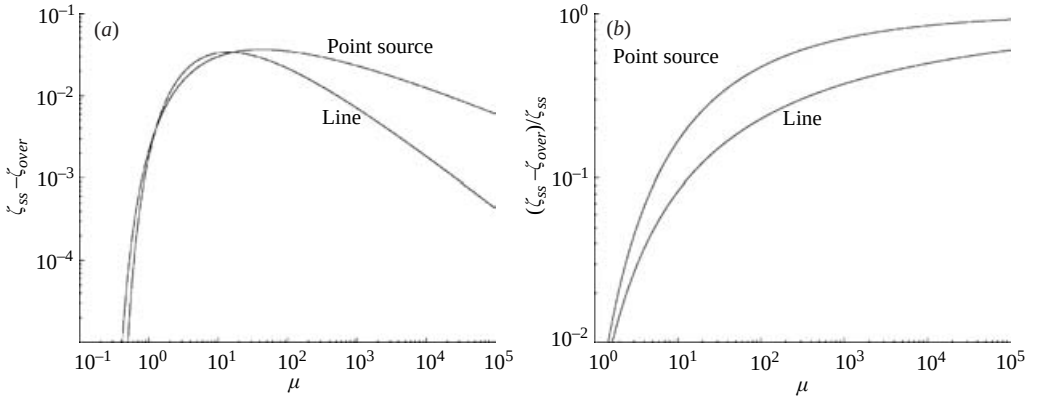

FIGURE 6. (*a*) $\zeta_{ss} - \zeta_{over}$ and (*b*) $(\zeta_{ss} - \zeta_{over})/\zeta_{ss}$, for both point-source and line plumes, as a function of μ.

steady-state value at the time of maximum overshoot, and this discrepancy increases with increasing μ.

The amplitude of the overshoot $(\zeta_{ss} - \zeta_{over})$ is depicted in figure 6(*a*) as a function of μ. For small values of μ no overshoot is predicted, but for larger values of μ the overshoot can be as high as 3.7% of the box height. The maximum overshoot is slightly higher for point-source plumes, 3.7%, and occurs at a higher value of $\mu_p \approx 41.4$ than for line plumes where the overshoot peaks at 3.4% at $\mu_l = 14.1$. The numerical solutions indicate no overshoot for *line* plumes when $\mu_l < \mu_{l.c} = 0.35$ and for *point*-source plumes when $\mu_p < \mu_{p.c} = 0.27$. A theoretical prediction for these values of μ_c is presented in § 2.3.

It is also informative to examine the depth of the ambient layer lost during the overshoot period and the time over which this loss is significant. The overshoot as a fraction of the steady-state ambient layer depth is shown in figure 6(*b*). Although the overshoot is only a small fraction of the box height, it can be a significant fraction of the ambient lower layer depth when the lower layer is thin (i.e. for large μ). This measure of overshoot becomes more significant as μ increases.

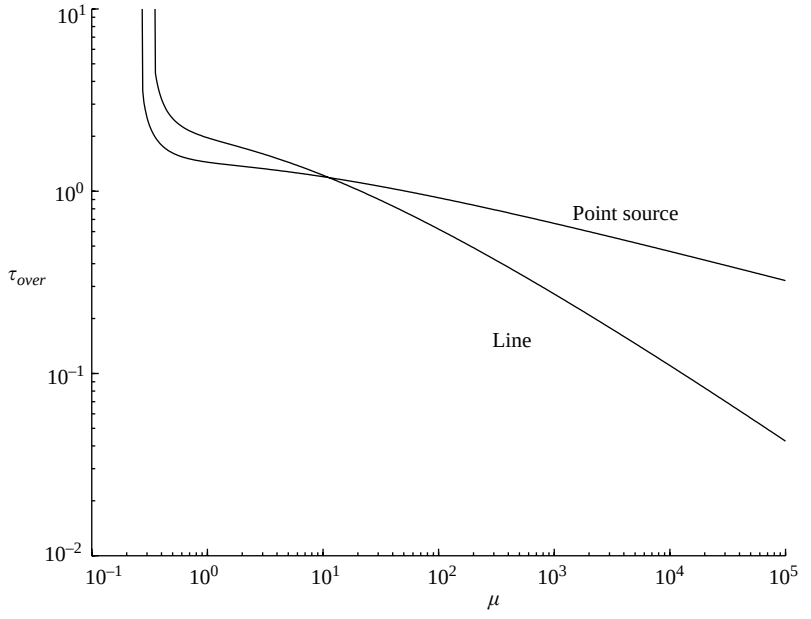

FIGURE 7. Time taken (τ_{over}) to reach ζ_{over} as a function of μ for point-source and line plumes.

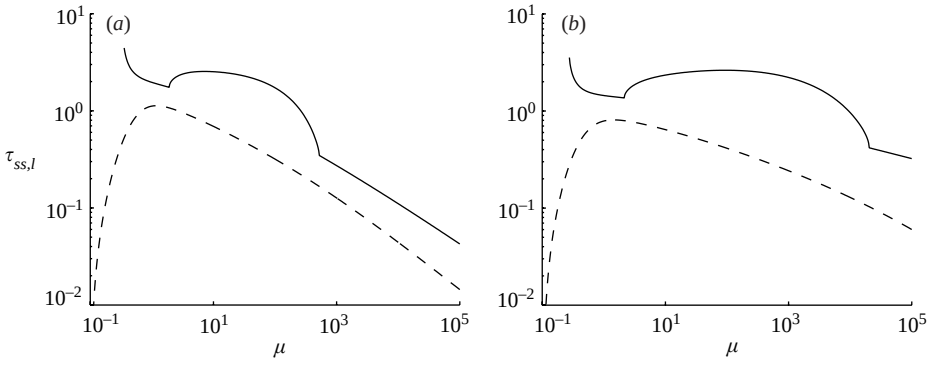

FIGURE 8. Time taken ($\tau_{ss,l}$) to reach the steady-state height during both the initial increase in layer depth (dashed line) and subsequent decay in layer depth towards the steady state (solid line) for line plumes (*a*) and point-source plumes (*b*).

Figure 7 shows the time, τ_{over}, taken to reach ζ_{over}. The near vertical slope at small μ indicates the approach of the singularity at the values of $\mu = \mu_c$ at which overshoot disappears. For $\mu > \mu_c$ the time to reach ζ_{over} decreases with increasing μ. It is somewhat counterintuitive that the time taken to establish a relatively deep peak layer (for larger μ) is less than that required to establish a relatively shallow layer. However, this is not inconsistent as we recall that μ is the ratio of the draining and filling timescales (see (2.15)) and thus for large μ the filling time is small relative to the draining time.

Figure 8 shows the time taken $\tau_{ss,l}$ to reach the steady-state layer depth. The dashed line in each plot is the time to reach ζ_{ss} the first time, i.e. as the interface descends.

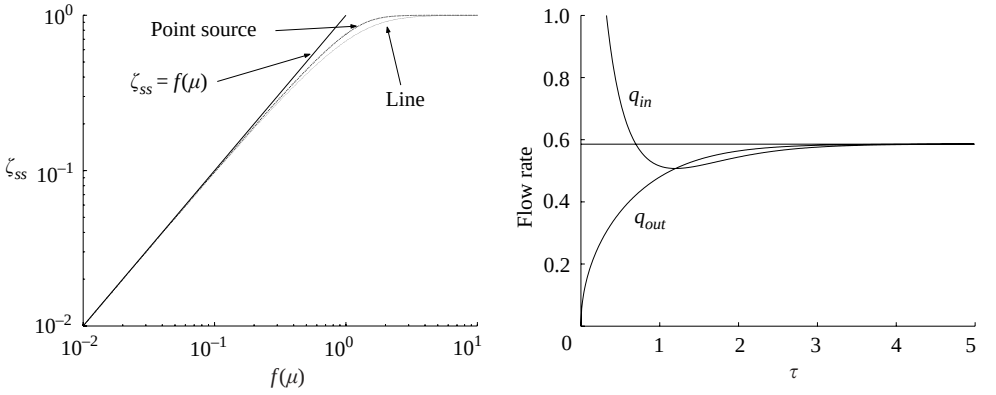

FIGURE 9. (*a*) ζ_{ss} for both point-source and line plumes as functions of $f(\mu) = \mu^{-2/3j}$. (*b*) $q_{in} = \sqrt{\mu}\zeta^{5/3}$ and $q_{out} = \sqrt{\delta(1-\zeta)}/\sqrt{\mu}$ against τ, for a point-source plume and $\mu = 10$. The horizontal line represents the value of the volume fluxes at the predicted steady state.

The solid line is the time taken to return to ζ_{ss} after overshooting, i.e. as the interface ascends. The upper and lower lines are similar, having a straightforward time offset, in all but two regions. Just above $\mu = \mu_c$, below which there is no overshoot, the time taken to return to the steady state increases dramatically with decreasing μ. This occurs because for μ close to μ_c overshoot is slight and at τ_{over} the volume and buoyancy fluxes, supplied to and draining from the buoyant layer, are very closely balanced. The ascent back to the steady-state layer depth is driven by the difference between these two closely balanced flows and, therefore, takes a longer time than less closely balanced flows. For $\mu < \mu_c$ there is no overshoot, and the layer merely increases to the steady layer depth.

The second difference occurs in the region of largest overshoot (figure 6). In this region the time taken to reach the peak is shorter than for smaller μ (figure 7), but as the overshoot is greater so is the time taken to ascend back to steady-state layer depth after overshoot. The sharp bounds at either end of the bulge (figure 8) are due to the definition of $\tau_{ss,l}$. When the overshoot is less than 1%, the value of $\tau_{ss,l}$ is the same as τ_{over}. However, when the overshoot is greater than 1% the value of $\tau_{ss,l}$ will diverge from τ_{over} because of the time taken to go from ζ_{ss} to ζ_{over} and back. Were, for example, 0.5% used as the steady-state criteria, the bulge would be wider, as the range of μ for which the overshoot is greater than 0.5% of the box height is greater than for 1%. The bulge would also be higher as the time taken to go from 0.5% overshoot to ζ_{over} and back would be greater. However, the sharp bounds to the bulge would remain.

Figure 9(*a*) shows the steady-state height for both line and point-source plumes as a function of $f(\mu) = \mu^{-2/3j}$. Based on the steady-state analytical predictions of (2.19) these two lines should approach the straight line $\zeta_{ss} = f(\mu)$, which is also plotted. Clearly the analytical solution and the numerical calculations closely agree for $f(\mu) < 10^{-1}$.

To clarify the steady-state balance between dimensionless flow rates into ($\sqrt{\mu}\zeta^{5/3}$) and out of ($\sqrt{\delta(1-\zeta)}/\sqrt{\mu}$) the buoyant layer (taken from the right-hand side of (2.12) with $j = 5/3$) we plot these volume flow rates as a function of time for a point-source plume with $\mu = 10$ (figure 9*b*). This shows the volume flow rate into the layer from the plume decreasing rapidly as the layer descends towards the plume source, and the flow rate out increasing gradually. The lines intersect at the point of maximum

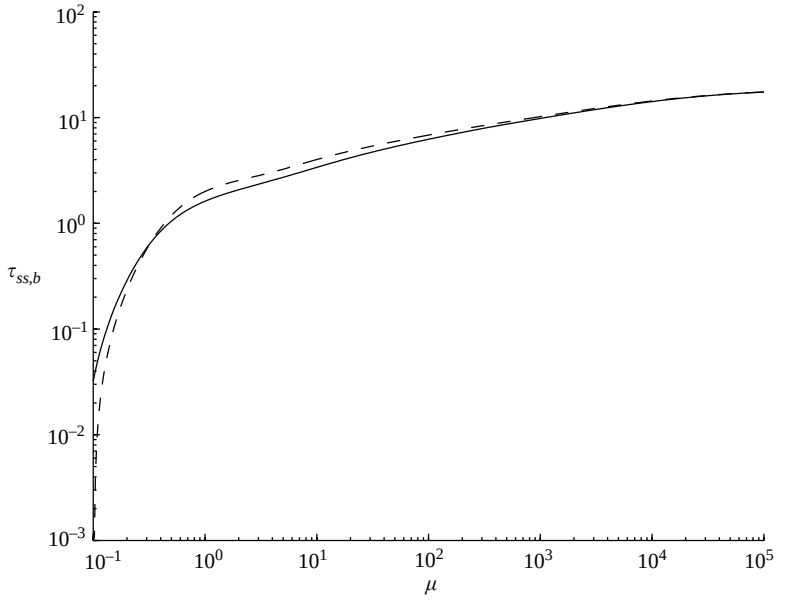

FIGURE 10. Plot of $\tau_{ss,b}$ as a function of μ. Dashed line for a point-source plume, and solid line for a line plume.

overshoot, after which the flow rate out exceeds the flow rate in and the layer thins as it approaches the steady state.

We also examine the time taken for the layer buoyancy to reach a steady state ($\tau_{ss,b}$), defined as the time taken for the buoyancy to reach 99% of the steady-state value. Values of $\tau_{ss,b}$ are shown in figure 10. Clearly $\tau_{ss,b}$ is considerably larger than $\tau_{ss,l}$ (see figure 8) for larger values of μ. When μ increases, ζ_{ss} decreases and, as a consequence, the volume flow rate into the upper layer decreases. The flow rate into the upper layer is therefore smaller, while the buoyancy of the upper layer required to balance the fluxes must increase. Consequently the buoyancy development lags behind the development of the layer thickness. As mentioned earlier, our model will overestimate the buoyancy of the upper layer as we assume a well-mixed layer. However, our results indicate that the development of the layer depth is much faster than the development of the layer buoyancy. This indicates that any errors in modelling the buoyancy development (such as our assumption of a well-mixed upper layer) will have only a minor effect on predictions of transient layer depth.

2.3. *Overshoot criteria*

One of the key questions that this model raises is under what circumstances will the buoyant layer overshoot the steady-state depth. To establish the value of μ at which overshoot first occurs, we draw an analogy with a mass–spring–damper system and the transition from over-damping to under-damping. This system can be written as a second-order linear ODE,

$$\ddot{x} + b\dot{x} + cx = 0 \tag{2.21}$$

where x denotes displacement from equilibrium. In matrix form this is

$$\begin{bmatrix} \dot{x} \\ \ddot{x} \end{bmatrix} = \begin{bmatrix} 0 & 1 \\ -c & -b \end{bmatrix} \begin{bmatrix} x \\ \dot{x} \end{bmatrix}. \tag{2.22}$$

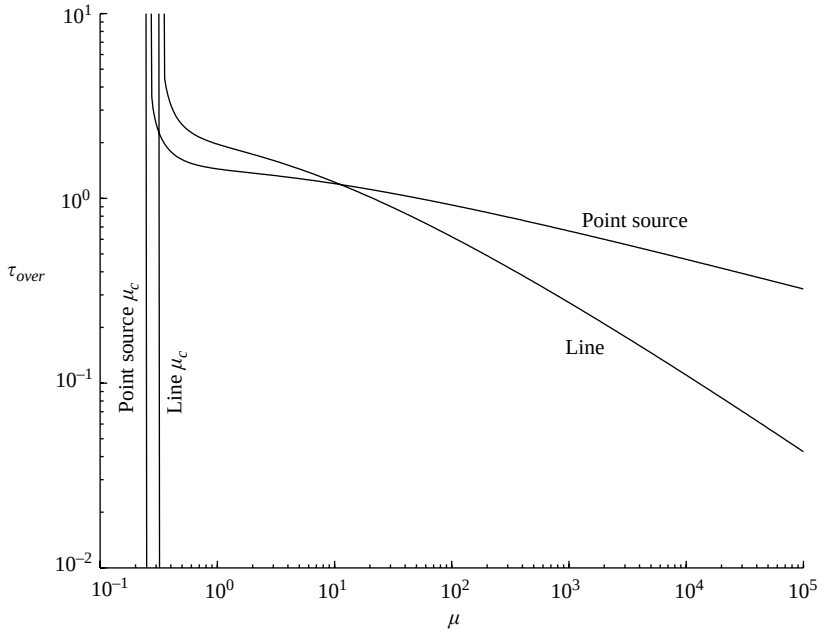

FIGURE 11. τ_{over} as a function of μ, for both point-source and line plumes. The vertical lines are μ_c taken from (2.25).

The eigenvalues of the matrix give the λ values of the full solution:

$$x = A_1 e^{\lambda_1 t} + A_2 e^{\lambda_2 t}. \tag{2.23}$$

The system is over-damped when λ_1 and λ_2 are real and distinct. The system is under-damped (implying overshoot of the equilibrium solution) when λ_1 and λ_2 are complex conjugates.

Examining a linearization of equations (2.12) and (2.13) about their steady-state values we obtain a similar equation:

$$\begin{bmatrix} \dot{\zeta} \\ \dot{\delta} \end{bmatrix} \approx \begin{bmatrix} \left.\dfrac{\partial \dot{\zeta}}{\partial \zeta}\right|_{\delta=\delta_{ss},\zeta=\zeta_{ss}} & \left.\dfrac{\partial \dot{\zeta}}{\partial \delta}\right|_{\delta=\delta_{ss},\zeta=\zeta_{ss}} \\ \left.\dfrac{\partial \dot{\delta}}{\partial \zeta}\right|_{\delta=\delta_{ss},\zeta=\zeta_{ss}} & \left.\dfrac{\partial \dot{\delta}}{\partial \delta}\right|_{\delta=\delta_{ss},\zeta=\zeta_{ss}} \end{bmatrix} \begin{bmatrix} \zeta - \zeta_{ss} \\ \delta - \delta_{ss} \end{bmatrix} = \begin{bmatrix} A & B \\ C & D \end{bmatrix} \begin{bmatrix} \Delta\zeta \\ \Delta\delta \end{bmatrix} \tag{2.24}$$

for any given value of μ and j.

Drawing an analogy with the mass–spring–damper system above, we calculate the eigenvalues of the matrix and establish the critical value of μ_c at which these eigenvalues become complex. A numerical search was used to establish the following result for point-source and line plumes respectively:

$$\begin{aligned} &\text{for } j = \tfrac{5}{3},\ \mu_{p.c} = 0.25, \\ &\text{for } j = 1,\ \mu_{l.c} = 0.32. \end{aligned} \tag{2.25}$$

For values of $\mu > \mu_c$ the eigenvalues are complex, implying that overshoot is possible. These values are very close to the values found through numerical integration of (2.12) and (2.13) and can be seen more clearly in figure 11.

Although there is not exact agreement, the use of the under-damping analogy helps to establish the region in which overshoot is likely to occur.

3. Experiments

We have now developed a full solution to the problem of time-dependent flow driven by an arbitrary number of equal plumes in an initially empty ventilated box. However, in order to complete this model, a number of simplifying assumptions have been made. The most significant of these is that the buoyant layer can be regarded as well-mixed throughout the transient, and that the plumes spread out in an infinitesimally thin layer when they first reach the top of the box. In order to verify whether or not these assumptions result in an accurate prediction of the front movement, a series of small-scale laboratory experiments were performed.

3.1. *Experimental technique*

The experiments were performed in a visualization tank of cross section $1.25\,\mathrm{m} \times 1.25\,\mathrm{m}$ that was filled to a depth of 1.5 m with fresh water. Two clear Perspex side panels of the tank allowed us to see the flow. A clear Perspex box of cross section $0.5\,\mathrm{m} \times 0.5\,\mathrm{m}$ and height 0.2 m was immersed in the visualization tank. A number of circular holes (18 of 3 cm diameter and 26 of 5 cm diameter) in the top and bottom of the box (the bottom also had one hole of 1 cm diameter and one of 0.5 cm) could be opened or closed by removing or adding plugs. This box design allows μ to be varied in the range $0.1 < \mu < 35$.

A salt solution was supplied to the box via a nozzle located in the centre of the top face, producing a descending turbulent saline plume inside the box. The nozzle was designed to produce a turbulent flow within one to two source diameters from the point of release (figures 6 and 7 of Hunt & Linden 2001). The nozzle, of exit diameter $D = 0.5\,\mathrm{cm}$, was mounted on a section of rigid plastic tubing. The vertical distance between the nozzle exit and the base of the box could be varied by raising or lowering the tubing before locking it into position with a grub screw. A constant volume flow rate of salt solution was achieved using a constant-head apparatus. The volume flow rate was measured using an in-line flowmeter and finely controlled with a needle valve. To distinguish between regions of fresh and salt solution a food dye was added to the plume and diffuse back-lighting used to light the experiments. A schematic of the experimental setup is shown in figure 12.

The density of the fresh water and the saline solution was measured using an Anton Paar DMA 35N density meter to an accuracy of $5 \times 10^{-4}\,\mathrm{g\,cm^{-3}}$. The typical ranges of plume source volume flow rates and reduced gravities were $2.0 < Q_{p.0} < 2.5\,\mathrm{cm^3\,s^{-1}}$ and $70 < g'_{p.0} < 150\,\mathrm{cm\,s^{-2}}$, respectively, giving buoyancy fluxes in the range $140 < B < 375\,\mathrm{cm^4\,s^{-3}}$. The virtual origin of the plume source was located using the technique presented by Hunt & Kaye (2001). The source conditions were characterized using the parameter Γ $(= (5/4\alpha)(Q_{p.0}^2 B / M_{p.0}^{5/2}))$ where $M_{p.0}$ is the source momentum flux. For a pure plume $\Gamma = 1$, but if there is an excess of momentum flux at the source the plume is considered to be forced (see Morton 1959). Conversely if there is a deficit of momentum at the source compared to a pure plume the source is regarded as lazy. The virtual origin was shown to be a function of the source radius and Γ by Hunt & Kaye (2001). For our experiments the source conditions lead to values in the range $0.8 < \Gamma < 1.5$ assuming an entrainment coefficient of $\alpha = 0.09$ and Gaussian profiles. In practice, volume flow rates and source buoyancies were chosen from the ranges above to keep Γ close to 1 in order to maintain a pure plume over the depth of the ambient layer. Therefore the virtual origin corrections for these experiments were in the range $0.9 < z_{avs} < 1.2\,\mathrm{cm}$ above the actual source. The origin correction z_{avs} then gives the corrected parameter $\widehat{\mu} = \widehat{H}^2 C^{3/2} / A^*$ where

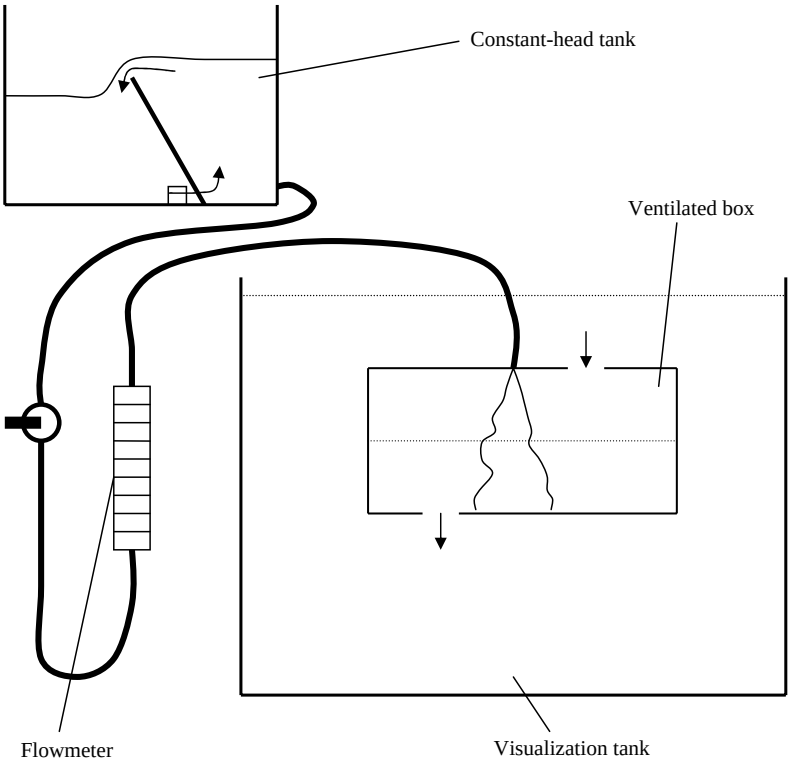

FIGURE 12. A schematic diagram of the ventilated box used in the experiments, showing the openings and the plume source.

$\widehat{H} = H + z_{avs}$. The corrected timescales $\widehat{T_d}$ and $\widehat{T_f}$ are also determined from (2.10) and (2.11) with H replaced by $\widehat{H}$. Similarly, the corrected ambient layer depth is given by $\widehat{\zeta} = (h + z_{avs})/\widehat{H}$. All measured values plotted have been corrected in this way, although for convenience the ˆ has been dropped from symbols on the plots.

An experiment was begun by first removing by hand the desired number of plugs from the upper and lower faces of the box. Any disturbances within the tank were allowed to dissipate. A tap was then opened, supplying salt solution to the nozzle; the needle valve was pre-set so that the desired flow rate was achieved immediately on opening the tap. The upper opening area was typically a factor of two greater than the lower opening area in order to maintain a low inlet velocity. This low inlet velocity prevents the inflowing jets of fluid from disturbing the interface, and enabled a sharp interface to be maintained. However, due to the geometry of the box, for smaller values of μ (larger vent areas) we were unable to maintain this ratio, resulting in disturbances on the interface that are discussed later.

3.2. *Observations*

3.2.1. *The initial transients*

A turbulent descending plume developed beneath the nozzle and on reaching the base of the box spread radially outwards as a saline current. The current spread to the box walls and a well-defined saline layer, with depth approximately equal to the width of the plume at the base of the box, was then clearly visible. The current

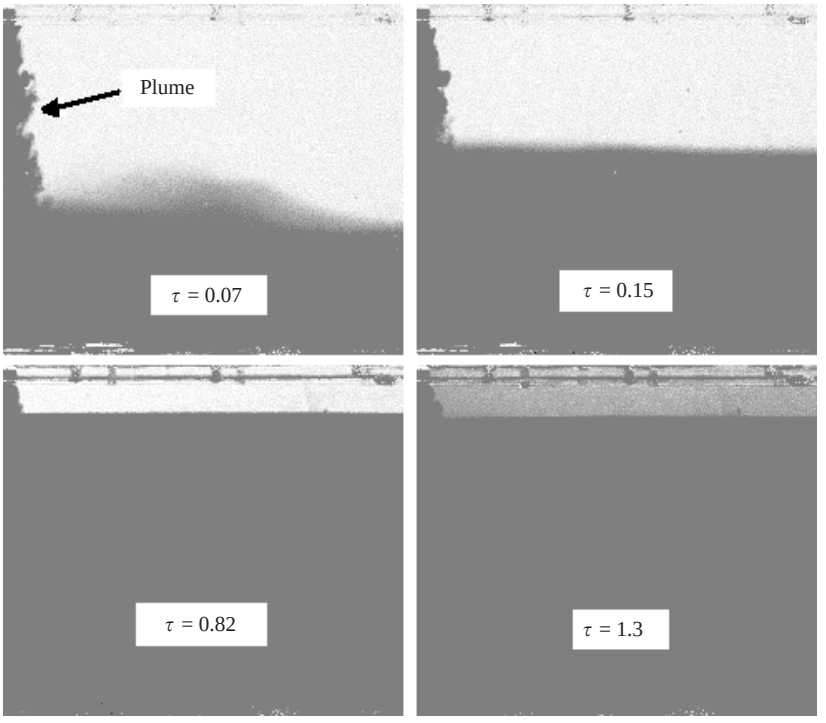

FIGURE 13. A series of four images taken from an experiment with $\mu = 34.5$. The left-hand side of each image coincides with the (dyed) plume centreline. The layer depth is seen to increase over time to a peak at $\tau = 0.82$ and then decrease slightly. The final image shows a slightly darker upper layer due to a small amount of mixing in the external ambient visualization tank. We estimated the buoyancy of this upper layer to be about 1% of the lower layer buoyancy.

was observed to slosh up the sidewalls of the box before slumping back downwards. This produced wave-like disturbances on the interface between the saline and fresh water layers, which propagated along the interface and were reflected off the sidewalls before gradually dissipating over time. The slumping also produced mixing between the layers. Once the slumping motion had settled down this mixing stopped and the only fluid crossing the density step was that entrained into the plume. Fluid from the saline layer drained through the openings in the base of the box and was replaced by fluid of ambient density passing in through the upper openings. The time origin $t = 0$ was taken as the instant when the plume collided with the floor of the ventilated box. This is in keeping with our model assumption that the plume spreads out in an infinitesimally thin layer, and the resulting initial conditions (2.20). The digital image analysis system DigiFlow (see Dalziel 1993) was used to track the position of the interface over time. In order to observe as stable an interface as possible only the vents on the left-hand side of the tank were opened, while the camera was pointed at the right-hand side of the tank. For most μ the disturbances on the interface due to the flow through the tank were minimal and were wave-like with no mixing across the interface and, therefore, had no effect on the interface height. However, for small μ the disturbances were more significant as discussed later in this section. Images taken from an experiment are shown in figure 13.

Although our model ventilated box allowed for μ values of up to $\mu = 35$, the volume of the visualization tank restricted the time over which we were able to run

experiments. As the saline solution drained out of the lower vent openings it formed a layer at the base of the visualization tank which deepened over time. Once this layer reached the base of the ventilated box we had to stop the experiment. We were therefore unable to reach the final steady state for $\mu > 10$. However, we were able to reach the peak layer depth, and these results are reported here. In a few experiments weak background motion in the visualization tank produced a discolouring of the background due to mixing with the lower layer. However, this mixing was determined to have negligible effect on the dynamics.

During the initial transients the saline layer rapidly increased in depth indicating that the draining rate was small compared with the rate of supply to the layer from the plume. The subsequent development of the stratification within the box was observed to be dependent on the opening area as described in (i) and (ii) below.

(i) For smaller openings ($\mu > 1$) the plume spread out and the buoyant layer initially deepened. The layer interface became horizontal and sharper as the initial slumping phase decayed away and the mixed fluid at the interface was entrained into the plume. The layer depth increased to a maximum and then decreased to the steady-state depth. Other than the finite thickness of the initial layer this is qualitatively in keeping with our model, and with the earlier work (Linden *et al.* 1990). During the initial plume outflow and slumping phases, mixing due to shear instabilities and weak overturning tended to smear and create disturbances on the interface, making accurate measurement of layer depths difficult. When measurements were made using DigiFlow a horizontal average of each time frame was taken (excluding the plume region), and the point of highest vertical gradient in the intensity (buoyancy) profile was taken to be the interface height. This allowed for a consistent definition for the interface height measurements over the course of each experiment and from experiment to experiment. However, before the layer interface sharpened some plume fluid remained above the reported interface height.

(ii) For sufficiently large opening areas ($\mu < 1$) a different flow regime was observed. Instead of the hydrostatic two-layer stratification modelled, the interface in the region below the open vents (the left-hand side of the box) was broken up and mixed by the jets of ambient fluid flowing through the vents. The interface on the right-hand side of the box, away from the openings, was also unstable, with waves persisting over the course of the entire experiment. There was also significant initial overshoot of the interface height due to these disturbances. The final average interface height was not observed to vary with μ and was of the order of the plume width at $z = H$. This flow regime was not observed by Linden *et al.* (1990) as their experiments covered a parameter range of $0.005 < A^*/H^2 < 0.055$ or $1.16 < \mu < 12.8$ (taking $C = 0.16$). However, we were able to run experiments over the broader range $0.14 < \mu < 34.5$.

Two main sets of data were obtained from our experiments: interface heights (peak and steady state) and time taken to reach the peak and steady-state heights. These are shown in figures 14 to 17.

The interface height data show good general agreement with the theory for $\mu > 1$, although the difference between peak and steady-state values from our experiments is less than that predicted. This is, in part, due to the smearing of the interface described earlier. As discussed above, we took the interface height to be the level at which the buoyancy step was steepest. This meant that there was always buoyant fluid above (that is, outside) the measured layer height. Over time the layer thinned (see figure 13), due to entrainment into the plume, and errors in ζ associated with this smearing were reduced. This means that the measurement of ζ_{over} will tend to underestimate the layer thickness and underestimate the extent of the overshoot. Despite this error we have

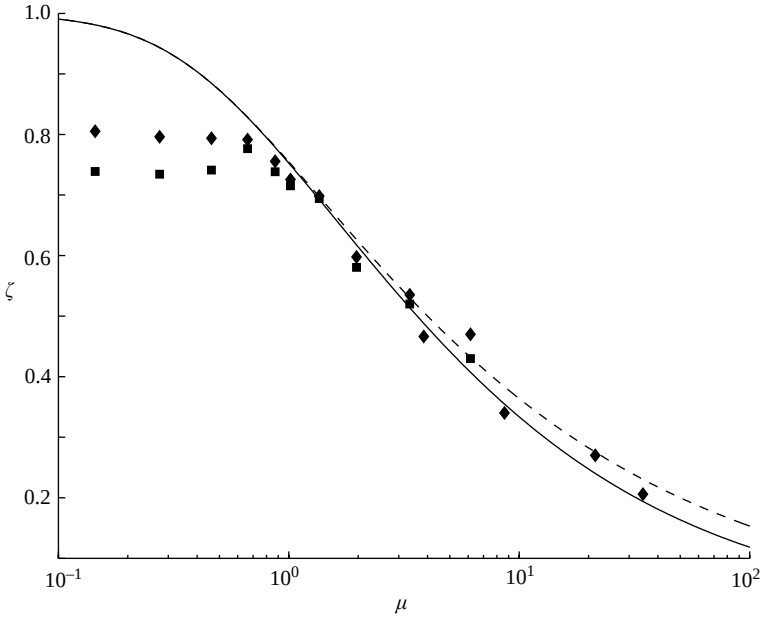

FIGURE 14. Experimental and theoretical values for ζ_{over} (diamonds and dashed line) and ζ_{ss} (squares and solid line). Note that for $\mu > 8$ we were unable to run the experiments for long enough to reach a steady state and therefore do not report steady-state interface heights for this range of μ. Note also that this figure is plotted using semi-log axes rather than the log-log axes used in some theoretical result figures.

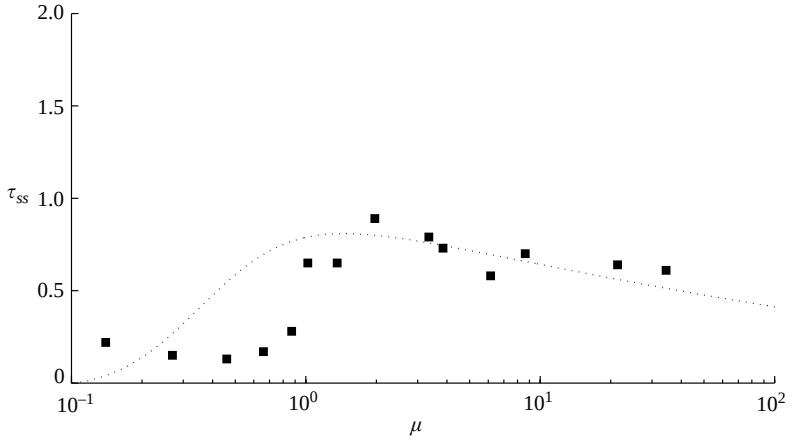

FIGURE 15. Theoretical and experimental values of τ_{ss}, the time taken for the interface to initially reach the steady-state height. Note that this figure is plotted using semi-log axes rather than the log-log axes used in some theoretical result figures.

continued to use the point of highest buoyancy gradient as the interface definition as it allows consistency over time.

For $\mu < 1$ the agreement is very poor and the observed flow differs from that expected for displacement ventilation flows. It is clear that once the flow breaks down, the interface height is no longer a function of μ. This flow regime actually results in the largest overshoot observed occurring at μ values where none is predicted.

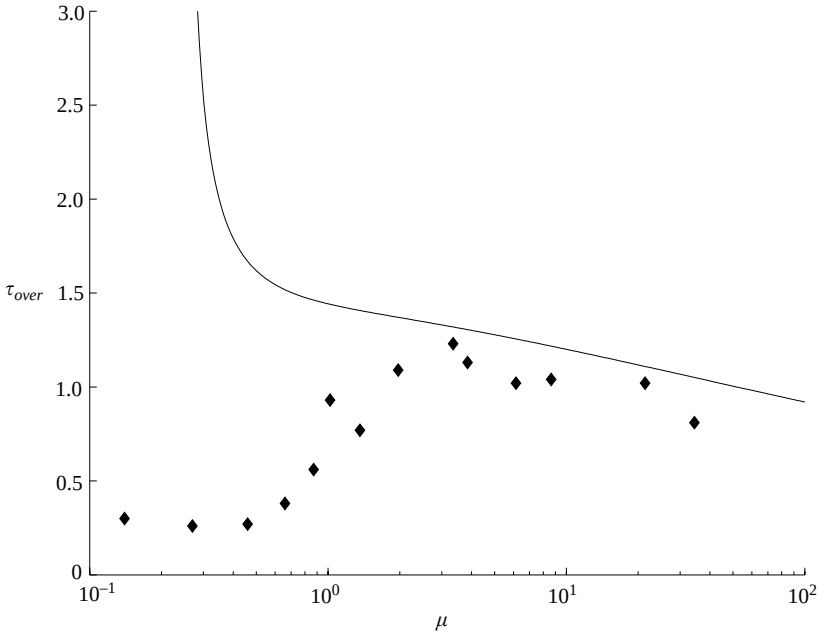

FIGURE 16. Theoretical and experimental values of τ_{over}, the time taken for the buoyant layer to reach its maximum depth. Note that this figure is plotted using semi-log axes rather than the log-log axes used in some theoretical result figures.

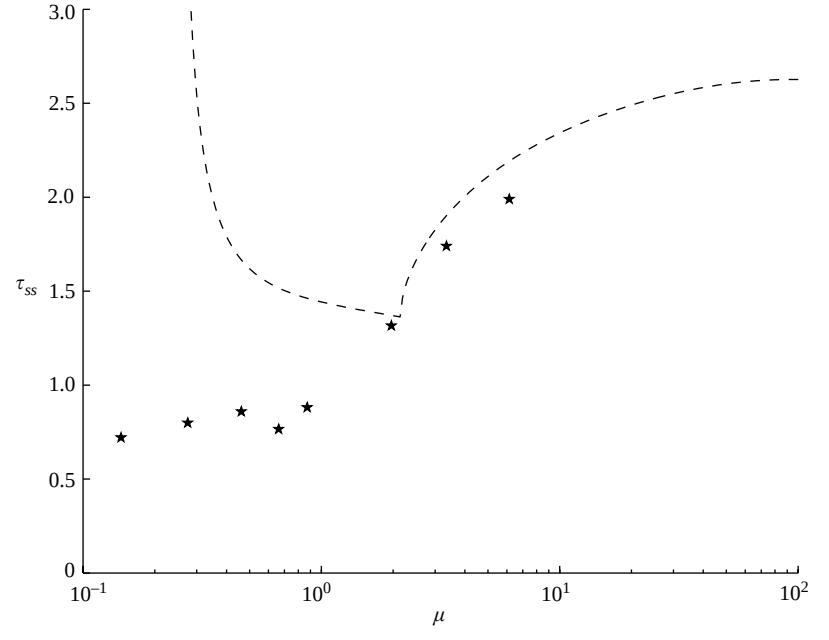

FIGURE 17. Theoretical and experimental values of τ_{ss}, the time taken for the interface to settle back to steady state. Note that for $\mu > 8$ we were unable to run the experiments for long enough to reach a steady state, and therefore do not report steady-state times in this range of μ. Note also that this figure is plotted using semi-log axes rather than the log-log axes used in some theoretical result figures.

Looking at the timescales (figures 15–17), we again see that for $\mu < 1$ there is poor agreement between theory and experiment due to the different flow regime observed. For larger values of μ the agreement improves. Two main reasons for these discrepancies are given, both linked with the very initial transients and associated mixing which are not accounted for in the model. First, a systematic error is associated with the measurement of the interface height at any time due to the smearing of the interface. The second source of discrepancy is also attributed to the initial transient interfacial mixing as this mixing increases the volume of fluid in the buoyant layer by entrainment from the layer at ambient density. This will tend to increase the rate at which the layer thickens and the interface rises, reducing the time taken to reach the peak and steady-state heights.

4. Conclusions

We have examined, using a combination of laboratory and theoretical modelling, the transient displacement flows that arise in ventilated boxes when there are sudden increases in buoyancy flux. Our results show that during the transient period the ventilation flow rates are less than those established in the steady state and that the buoyant upper layer can exceed (or overshoot) the steady-state layer depth.

The transients leading to the steady state are governed by the draining (T_d) and filling (T_f) times, and the dimensionless parameter $\mu = T_d/T_f$. The parameter μ is equivalent to the dimensionless opening area A^*/H^2 identified by Linden *et al.* (1990). Our formulation provides an alternative interpretation of this parameter. Rather than being a geometric statement it characterizes the balance between filling and draining flows. For large values of μ the draining time is larger than the filling time. Therefore the box will be fuller before the draining flow can balance the filling flow, resulting in the buoyant layer being deeper. For small μ the draining time is smaller and the buoyant layer is thinner.

We have also demonstrated the possibility of the layer depth overshooting its steady-state depth. This behaviour is also controlled by the parameter μ. For $\mu > \mu_c$ overshoot will occur. We calculated this value for point-source and line plumes by numerical integration of the transient equations. These values were compared to a theoretical calculation based on drawing an analogy between this system and a spring–mass–damper system. These two values showed good agreement and indicate that one should expect overshoot for $\mu > 0.35$ for line plumes and $\mu > 0.27$ for point-source plumes.

Salt-bath experiments were performed to verify the key theoretical findings. We measured the peak and steady-state interface heights and the time taken to reach both these heights. The experimental results showed good agreement with our theoretical predictions for $\mu > 1$. However, below this value, the finite thickness of the outflow from the plume and the large volume flow rate through the box meant that a constant-thickness layer was measured and found to be independent of μ. This constant-thickness regime has not previously been identified due to a lack of experimental results for small μ. Although we have identified this new flow regime, more work is required to fully understand this behaviour.

The authors gratefully acknowledge the financial support of BP through their Advanced Energy in Buildings Programme at Imperial College London.

Appendix A. Generalized plume scalings

The volume flux Q_p and buoyancy g'_p of a self-similar turbulent plume can be written in terms of powers of the buoyancy flux B, the height z above the source, a lengthscale L associated with the source, and a constant C_k that is a function of the plume entrainment coefficient α_k and source geometry. In the most general form this yields

$$Q_p = C_k B^i z^j L^k, \tag{A 1}$$

$$g'_p = \frac{B}{Q_p} = C_k^{-1} B^{1-i} z^{-j} L^{-k}. \tag{A 2}$$

Dimensional arguments can then be used to establish relationships between the exponents i, j and k. The dimensions of Q_p and B are given by $[Q_p] = l^3 t^{-1}$ and $[B] = l^4 t^{-3}$ which leads to

$$i = \tfrac{1}{3}, \qquad j + k = \tfrac{5}{3}. \tag{A 3}$$

Two significant cases are worth noting. When $j = \frac{5}{3}$ and $k = 0$ we obtain the standard scaling for a point-source plume:

$$Q_p = C_0 B^{1/3} z^{5/3} \tag{A 4}$$

(see Morton, Taylor & Turner 1956), and when $j = 1$, $k = \frac{2}{3}$ we obtain the case of a line plume for which the volume flux per unit length (Q_p/L) may be expressed in terms of the buoyancy flux per unit length (B/L) as

$$\frac{Q_p}{L} = C_{2/3} \left(\frac{B}{L}\right)^{1/3} z. \tag{A 5}$$

In this case L is the length of the line plume. The use of these generalized scalings enables the development of a single set of equations governing the time-dependent displacement flows, which can then be solved for different values of j and k, rather than deriving the equations for line and point-source plumes separately.

Expressions for C_k are determined by solving the conservation equations for the point-source and line plumes. They are given respectively by

$$C_0 = \pi \left(\frac{5}{2\pi\alpha_0}\right)^{1/3} \left(\frac{6\alpha_0}{5}\right)^{5/3}, \qquad C_{2/3} = \left(2\alpha_{2/3}\right)^{2/3}. \tag{A 6}$$

In this paper the experimental results are scaled using an entrainment coefficient of $\alpha_0 = 0.09$ which results in a value of $C_0 = 0.16$. We did not use line plumes in our experiments.

Appendix B. Initial values

Writing $\zeta = \zeta_0 + \zeta'$, $\delta = \delta_0 + \delta'$, and $\tau = \tau_0 + \tau'$ we obtain

$$\frac{\mathrm{d}\delta}{\mathrm{d}\tau} \approx \frac{\delta'}{\tau'} \approx \frac{1 - (1 - \sqrt{\mu}\tau')^j (1 + \delta')}{1 - (1 - \sqrt{\mu}\tau')}. \tag{B 1}$$

In the limit as $\tau' \to 0$ we obtain

$$\frac{\mathrm{d}\delta}{\mathrm{d}\tau} = \frac{j}{2}\sqrt{\mu} \quad \text{at} \quad \tau = 0. \tag{B 2}$$

REFERENCES

Baines, W. D. & Turner, J. S. 1969 Turbulent buoyant convection from a source in a confined region. *J. Fluid Mech.* **37**, 51–80.

Cooper, P. & Linden, P. F. 1996 Natural ventilation of an enclosure containing two buoyancy sources. *J. Fluid Mech.* **311**, 153–176.

Dalziel, S. B. 1993 Rayleigh-Taylor instability: experiments with image analysis. *Dyn. Atmos. Oceans* **20**, 127–153.

Gladstone, C. & Woods, A. W. 2001 On buoyancy-driven natural ventilation of a room with a heated floor. *J. Fluid Mech.* **441**, 293–314.

Holford, J. M. & Hunt, G. R. 2001 The dependence of the discharge coefficient on density contrast – experimental measurements. In *Proc. 14th Australasian Fluid Mech. Conf., 9–14 December 2001* (ed. B. B. Dally), pp. 123–126. University of Adelaide.

Hunt, G. R. & Holford, J. M. 2000 The discharge coefficient – experimental measurement of a dependence on density contrast. In *Proc. 21st Intl AIVC Conf., 26–29 September*, The Hague, pp. 12–24. Air Infiltration and Ventilation Centre, Document AIC-PROC-21-2000.

Hunt, G. R. & Kaye, N. G. 2001 Virtual origin correction for lazy turbulent plumes. *J. Fluid Mech.* **435**, 377–396.

Hunt, G. R. & Linden, P. F. 2001 Steady-state flows in an enclosure ventilated by buoyancy forces assisted by wind. *J. Fluid Mech.* **426**, 355–386.

Linden, P. F. & Cooper, P. 1996 Multiple sources of buoyancy in a naturally ventilated enclosure. *J. Fluid Mech.* **311**, 177–192.

Linden, P. F., Lane-Serff, G. F. & Smeed, D. A. 1990 Emptying filling boxes, the fluid mechanics of natural ventilation. *J. Fluid Mech.* **212**, 309–335.

Manins, P. C. 1979 Turbulent buoyant convection from a source in a confined region. *J. Fluid Mech.* **91**, 765–781.

Morton, B. R. 1959 Forced plumes. *J. Fluid Mech.* **5**, 151–163.

Morton, B. R., Taylor, G. I. & Turner, J. S. 1956 Turbulent gravitational convection from maintained and instantaneous sources. *Proc. R. Soc. Lond.* A **234**, 1–23.

Sandberg, M. & Lindstrom, S. 1990 Stratified flow in ventilated rooms – a model study. In *Proc. ROOMVENT '90: 2nd Intl Conf. on Air Distribution in Rooms, Oslo, Norway, 13–15 June.* NORSK VVS, P. Box 5042, Majorstua 0301, Oslo.

Wong, A. B. D., Griffiths, R. W. & Hughes, G. O. 2001 Shear layers driven by turbulent plumes. *J. Fluid Mech.* **434**, 209–241.

Worster, M. G. & Huppert, H. E. 1983 Time-dependent density profiles in a filling box. *J. Fluid Mech.* **132**, 457–466.